THE WEAK-BEAM TECHNIQUE AS APPLIED TO DISSOCIATION MEASUREMENTS

D. Cockayne

THE WEAK-BEAM TECHNIQUE AS APPLIED TO DISSOCIATION MEASUREMENTS

D. J. H. COCKAYNE

Electron Microscope Unit, University of Sydney,
N. S. W., 2006, Australia

Résumé. — La méthode du faisceau faible en microscopie électronique est appliquée à la mesure de la séparation des dislocations partielles. On analyse la précision des résultats expérimentaux obtenus, et on envisage l'ensemble des hypothèses utilisées pour en déduire des valeurs de l'énergie de faute d'empilement γ.

Abstract. — The application of the weak-beam method of electron microscopy to the measurement of the separation of partial dislocations $\gtrsim 2.0$ nm is discussed. The accuracy of the experimental results is analysed, and approximations in obtaining values of the stacking-fault energy, γ, are outlined.

1. **Introduction.** — The weak-beam method of electron microscopy [1] is the most powerful method available for studying the detailed geometry of individual lattice defects. It enables the positions of dislocation cores to be determined to an accuracy of better than 1 nm, and allows the geometry of dislocation interactions to be studied with greatly increased resolution compared with previous electron microscope methods. For this reason, determinations of stacking-fault energies using the dimensions of defect configurations, such as the measurement of the dissociation of Shockley partial dislocations and the size of extended nodes, can be made more accurately and for smaller defects than with other methods. In this paper the application of the method to the determination of stacking-fault energies by measuring the dissociation of Shockley partial dislocations is discussed.

2. **Role of electron microscopy in determining γ.** — A direct method of determining the stacking-fault energy in a material which crystallises with the f. c. c. or h. c. p. structure is to measure the separation of Shockley partial dislocations. Assuming that the partials can be regarded as singular Volterra type dislocations, i. e. without taking into account their core structures, the force per unit length, F, between two straight partials can easily be calculated using anisotropic or isotropic elasticity ; it is found to be $F = Kb_p^2/r$, where r is the separation of the partials, b_p is the magnitude of the partial Burgers vectors, and K is a function of the orientation of the dislocation line and of the elastic constants. In the isotropic case [2]

$$K = \frac{\mu}{8\pi}\left(\frac{2-\nu}{1-\nu}\right)\left(1 - \frac{2\nu\cos 2\alpha}{2-\nu}\right)$$

where μ is the shear modulus, ν is the Poisson ratio and α is the angle between the total Burgers vector and the dislocation line. The stacking-fault energy, γ, is then determined from the equilibrium condition $F = \gamma$.

In this situation the problem facing electron microscopy is to determine r, the separation of the partials. In normal bright- or dark-field electron microscopy, two difficulties arise. Firstly, the image width of a dislocation line is approximately $\xi_g/3$ where ξ_g is the extinction distance for the reflection concerned. For a typical case in metals, this results in image widths $\approx$ 10 nm, which makes it difficult to resolve the images of two (partial) dislocations which have $r \lesssim 10$ nm. Secondly, the image position only approximately defines the position of the dislocation core. These difficulties can be overcome to some extent by using computer simulated images (for a review, see [3]), but ultimately, when $r \lesssim 8$ nm (e. g. in Cu, Au, Ag, Si, Ge) the images are insufficiently sensitive to variations in r to make this method practical.

A number of alternative methods involving defects with more complex geometry have been used to overcome these difficulties. In particular, the method of measuring the radius of curvature, R (or inside dimensions, W) of extended nodes [4, 5] is of advantage because the images of the partials are more easily resolved at the node. However this method is subject to a number of difficulties : (i) in practice, nodes are rarely symmetrical or of a uniform size, making it difficult to determine R (or W) ; (ii) the relationships between γ and the geometrical parameters of the node are not as well-defined as for the separation of Shockley partial dislocations.

3. **Images using the weak-beam method.** — The weak-beam method of electron microscopy [1] enables the difficulties outlined above to be overcome in two

respects. Firstly, each partial dislocation produces an image peak whose half-width is approximately 1.5 nm ; and secondly, the positions of the image peaks define the positions of the partials to an accuracy of $\approx$ 0.7 nm.

Weak-beam images are obtained by forming a (dark-field) image using a first order Bragg reflection for which the perfect crystal is oriented far from the Bragg reflecting condition. This is in contrast to normal images for which the crystal is oriented close to the Bragg reflecting condition. The difference between the two types of image is seen in figure 1, for dislocations in silicon. The theoretical principles of the method have been analysed and the experimental conditions necessary to obtain a given level of accuracy in the determination of dislocation core positions have been defined [6].

4. **Accuracy of determination of dislocation line positions.** — To determine how the positions of image peaks (e. g. in Fig. 1) are related to dislocation core positions, weak-beam images have been computed using many-beam dynamical theory, taking absorption into account. Figure 2 shows some examples, and it is observed that the image peak lies to one side of the dislocation core. If we were to assume that the position of the image peak lies at the position of the projection of the dislocation core on the image plane, then, for the cases shown, there would be an error of approximately 2 nm in the determination of the core position. However this assumption is not necessary, because there are a number of ways to predict the displacement of the image peak from the dislocation core position :

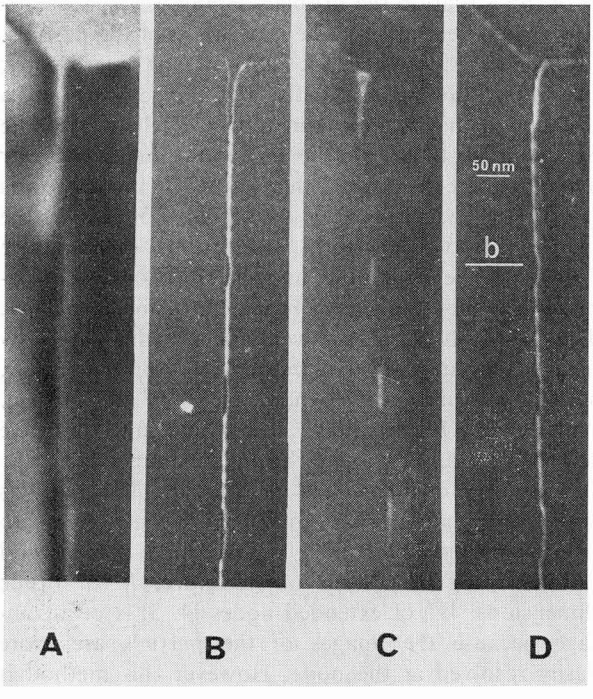

FIG. 1. — A constricted dislocation in silicon imaged under various diffracting conditions : *a*) A strong-beam $2\bar{2}0$ dark-field image, in which the constricted segments and node extension are masked. *b*) A weak-beam $2\bar{2}0$ dark-field image showing both partial dislocations. *c*) A weak-beam $11\bar{1}$ dark-field image, giving $\mathbf{g}.\mathbf{b} = 0$ for the total Burgers vector, showing the stacking-faults imaged at the extended node and at the « bowed » dislocation segments. *d*) A weak-beam $0\bar{2}2$ dark-field image, in which the partial dislocation with Burgers vectors $a/6\ [2\bar{1}\bar{1}]$ is out of contrast. (From Ray and Cockayne [11] by courtesy of the Royal Society.)

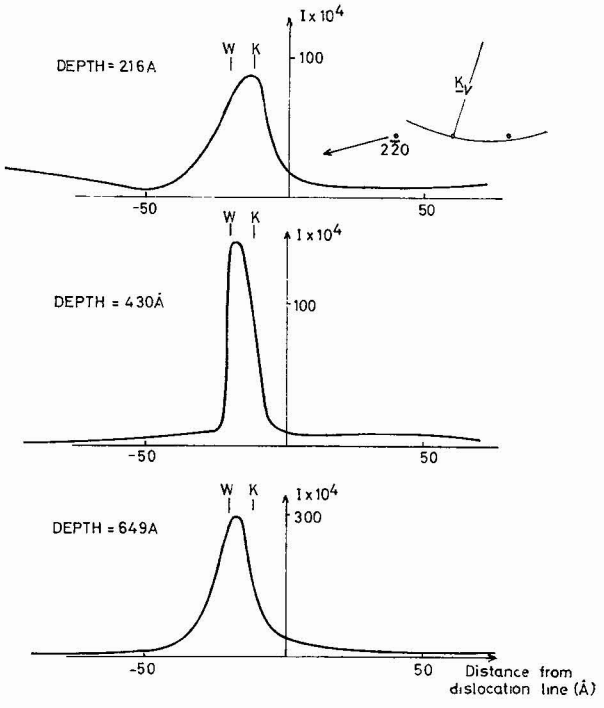

FIG. 2. — Computed weak-beam images of an undissociated edge dislocation in copper at various depths (as indicated) in a foil of thickness $2\,\xi_g$. Parameters : $\mathbf{g}.\mathbf{b} = 2$; $\mathbf{g} = 220$; 6 beam calculation ; 100 kV electrons ; isotropic elasticity ; $s_g = -0.25\ \text{nm}^{-1}$. W is the image peak position predicted by eq (4.1), and K by eq. (4.2).

(1) To a first approximation, the image peaks arise from regions in the lattice where the strain field of the defect bends the lattice planes locally into the Bragg reflecting condition. This assumption results in the prediction that (for isotropic elasticity) the image peak lies at a distance

$$X_W = \frac{-\,\mathbf{g}.\mathbf{b}}{2\,\pi s_g}\left(1 + \frac{\kappa}{2(1-\nu)}\right) \qquad (4.1)$$

from the projection of the dislocation core, where $\kappa = 1$ for an edge dislocation and 0 for a screw dislocation, and s_g is the distance of the Ewald sphere from the reciprocal lattice point g. This position is marked W in figure 2.

(2) On the other hand it can be argued that for the conditions which are used in obtaining weak-beam images, the kinematical theory should be a good approximation for predicting the image peak position. If we use the approach of Hirsch, Howie and Whe-

lan [7] to describe the average kinematical image (i. e. the distance between the centres of the initial and final circles on the amplitude-phase diagram), then the image peak position (for the case $\mathbf{g}.\mathbf{b} = 2$ - other cases can also be obtained from (7)), is given by

$$X_K = \frac{-2.1}{2\pi s_g}\,(\text{edge}); \qquad X_K = \frac{-1.0}{2\pi s_g}\,(\text{screw}). \quad (4.2)$$

This position is marked K in figure 2.

To determine which, if either, of these equations gives a satisfactory description of the distance of the image peak from the projection of the dislocation line, the positions predicted by the two equations were compared with images such as those in figure 2. It was found that for first order reflections with $|s_g| \gtrsim 0.2\ \text{nm}^{-1}$ and $\mathbf{g}.\mathbf{b} \leqslant 2$:

(i) The calculated image peak positions lay between the two positions given by eq. (4.1) and (4.2) the exact position of the peak depending on foil thickness and dislocation depth.

(ii) For this value of $|s_g|$ the difference between X_W (eq. (4.1)) and X_K (eq. (4.2)) is about 1 nm so that either equation can be used to deduce the position of the dislocation core to an accuracy of $\approx$ 1 nm (for $|s_g| \gtrsim 0.2\ \text{nm}^{-1}$).

These conclusions are supported by figure 3, where the computed peak positions for undissociated edge

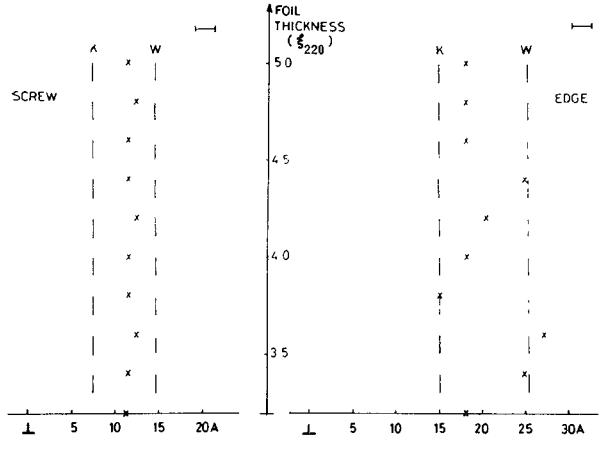

FIG. 3. — Computed weak-beam image peak positions for edge and screw dislocations in copper. The peak positions lie between the positions predicted by eq. (4.1) (W) and (4.2) (K). Parameters : $|\mathbf{g}.\mathbf{b}| = 2$; 6 beam calculations ; 100 kV electrons ; isotropic elasticity.

and screw dislocations in copper are plotted as a function of foil thickness. W and K are the peak positions predicted by equations (4.1) and (4.2) respectively. (The relationship between these equations, and the approximations involved in their derivation from the dynamical theory, have been discussed by De Ridder and Amelinckx [8] and Cockayne [6].) In figure 4 (D. Saldin unpublished) images have been calculated for two diffraction geometries (see figure

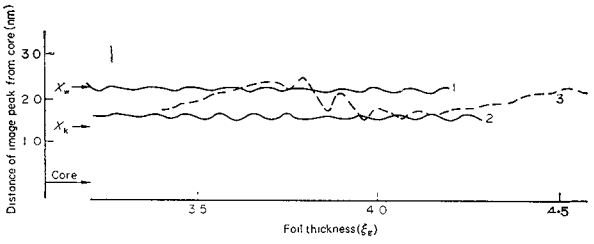

FIG. 4. — A plot of the weak-beam image peak positions as a function of foil thickness for an undissociated edge dislocation in copper. It is seen that the peak position lies between the positions predicted by eqs. (4.1) (X_W) and (4.2) (X_K). Parameters : $|\mathbf{g}.\mathbf{b}| = 2$; 6 beam calculation ; 100 kV electrons ; isotropic elasticity. Curve 1, dislocation depth = 2.20 ξ_g ; $g = \bar{2}\bar{2}0$; $s_g = -0.24\ \text{nm}^{-1}$; Curve 2, dislocation depth = 1.56 ξ_g ; $\mathbf{g} = \bar{2}20$; $s_g = -0.25\ \text{nm}^{-1}$; Curve 3, dislocation depth = 2.2 ξ_g ; $\mathbf{g} = 220$; $s_g = +0.24\ \text{nm}^{-1}$.

caption) and the image peak positions plotted as a function of foil thickness. For both diffraction geometries, the image peak position lies (effectively) between X_W and X_K and is seen to vary periodically with foil thickness (period = $0.095\ \xi_{220} \approx 1/|s_g|$). (This periodicity can be compared with the beat frequency between Bloch waves on branches 2 and 4 of the dispersion surface, numbering from the top of the dispersion surface.)

These considerations lead to the conclusion that for $|s_g| \gtrsim 0.2\ \text{nm}^{-1}$ the weak-beam image of a dislocation with $\mathbf{g}.\mathbf{b} \leqslant 2$ is :

(i) Close to ($\lesssim$ 2 nm from) the projection of the dislocation core ;

(ii) Sufficiently narrow ($\approx$ 1.5 nm at half height) to enable its position to be accurately defined experimentally ;

(iii) At a position which is relatively insensitive (to $\approx$ 1 nm) to foil thickness and dislocation depth, and given to an accuracy of better than 1 nm by eq. (4.1).

The insensitivity of the image peak position mentioned in (iii) above is governed by a restriction on w ($= s_g\,\xi_g$), and the criterion $|w| = |s_g\,\xi_g| \gtrsim 5$ appears to be a minimum requirement in this regard [6]. In summary it can be stated that, for dislocations, the use of eq. (4.1) for analysis of first order weak-beam images with $\mathbf{g}.\mathbf{b} \leqslant 2$ will give an accuracy of better than 1 nm for determining dislocation core positions provided $|s_g| \gtrsim 0.2\ \text{nm}^{-1}$ and, simultaneously, $|w| = |s_g\,\xi_g| \gtrsim 5$.

5. **Measurement of Shockley partial separations.** — With this appreciation of the accuracy of weak-beam images for determining dislocation core positions, we can now consider its application to determining partial separations. We consider the dislocation reaction in an f. c. c. material

$$\mathbf{b} = \tfrac{1}{2}[1\bar{1}0] \rightarrow \tfrac{1}{6}[1\bar{2}1] + \tfrac{1}{6}[2\bar{1}\bar{1}]$$

for an edge dislocation parallel to $[11\bar{2}]$ in a foil with normal [111]. We have $\mathbf{g}.\mathbf{b}_1^p = \mathbf{g}.\mathbf{b}_2^p = 1$ for both partials if $\mathbf{g} = 2\bar{2}0$, where $\mathbf{b}_1^p$ and $\mathbf{b}_2^p$ are the Burgers vectors of the partial dislocations. There is then no stacking-fault contrast. As in the case of an undissociated dislocation, we can predict that there will be two image peaks, one close to each of the partials, and this is in accord with earlier kinematical calculations [9]. The prediction is verified for partial separations $\gtrsim$ 2.0 nm by computed many-beam images (examples of which are shown in figure 5). In general one partial shows a higher intensity peak than the other, because of the asymmetry of the strain field between and outside the partials, the relative intensities of the two changing with the sign of the g-vector.

From figure 5 and similar images, it is evident that the partial separation Δ can be equated with the

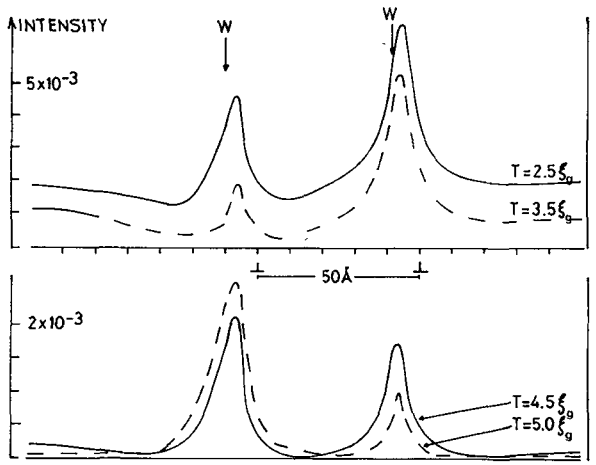

FIG. 5. — Computed weak-beam images of a dissociated edge dislocation in copper lying at depth ξ_{220} in (111) foils of various thickness, T, as indicated. W are the image peak positions predicted using eq. (5.1). The images are for

$$\mathbf{g} = 2\bar{2}0, \mathbf{b} = \frac{1}{2}[1\bar{1}0] \rightarrow \frac{1}{6}[1\bar{2}1] + \frac{1}{6}[2\bar{1}\bar{1}], \mathbf{u} = \frac{1}{\sqrt{6}}[11\bar{2}],$$

$|s_g| = 0.2$ nm^{-1} and unit incident beam intensity.

image peak separation Δ_{obs} to an accuracy of better than $\approx$ 1.0 nm. However we can identify two effects which cause Δ_{obs} and Δ to differ :

(i) The image peak positions and Δ_{obs} vary about mean values with dislocation depth and foil thickness. This can be overcome to a great extent by taking an average over images for different thicknesses and defect depths.

(ii) There is a difference between Δ and the mean value of Δ_{obs} due to the fact that the mean positions of the image peaks are not equidistant from the respective dislocation cores. A method for allowing for this is to make the assumption discussed above, that the image peaks occur for those positions of the lattice where the strain field orients the lattice into the Bragg reflecting condition for the particular reflection used to form the weak-beam image. This criterion corresponds to the statement that the image taken in a reflection $\mathbf{g}$ will have an intensity peak at any point in the image corresponding to a column in the crystal within which $[s_g + (\mathrm{d}/\mathrm{d}z)(\mathbf{g}.\mathbf{R})] = 0$ at a turning point of $(\mathrm{d}/\mathrm{d}z)(\mathbf{g}.\mathbf{R})$, where $\mathbf{R}$ is the lattice displacement in the column.

As an example of this analysis, we consider the coordinate system shown in figure 6 for which

$$\mathbf{g}.\mathbf{R}_i^p = \frac{\mathbf{g}.\mathbf{b}_i^p}{2\pi}\left(\theta_i + \frac{\sin 2\theta_i}{4(1-\nu)}\right)$$

([10], p. 251), since $\mathbf{g}.(\mathbf{b}_i^p \wedge \mathbf{u}) = 0$, where

$$\mathbf{R} = \mathbf{R}_1^p + \mathbf{R}_2^p .$$

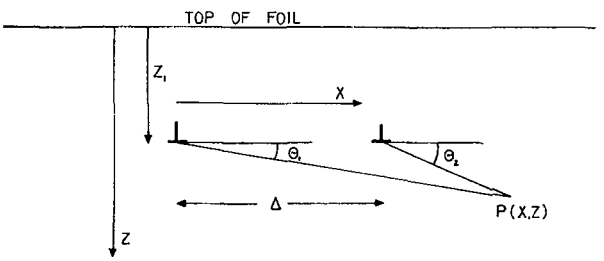

FIG. 6. — Coordinates used in text to describe the displacement at point P.

The turning point of $(\mathrm{d}/\mathrm{d}z)(\mathbf{g}.\mathbf{R})$ for any particular value of x occurs at $z = Z_1$. The condition that

$$[s_g + (\mathrm{d}/\mathrm{d}z)(\mathbf{g}.\mathbf{R})] = 0$$

at a turning point of $(\mathrm{d}/\mathrm{d}z)(\mathbf{g}.\mathbf{R})$ then gives

$$-s_g = \frac{\mathbf{g}.\mathbf{b}_1^p}{2\pi x}\left(1 + \frac{1}{2(1-\nu)}\right) + \frac{\mathbf{g}.\mathbf{b}_2^p}{2\pi(x-\Delta)}\left(1 + \frac{1}{2(1-\nu)}\right)$$

$$= \frac{\mathbf{g}.\mathbf{b}^p}{2\pi}\left(1 + \frac{1}{2(1-\nu)}\right)\left(\frac{1}{x} + \frac{1}{(x-\Delta)}\right)$$

since $\mathbf{g}.\mathbf{b}_1^p = \mathbf{g}.\mathbf{b}_2^p$. The two solutions for x, which are the predicted positions of the two weak-beam image peaks, are

$$x = (2 + c\Delta \pm \sqrt{(4 + c^2\Delta^2)})/2c \qquad (5.1)$$

where

$$c = -s_g \Big/ \frac{\mathbf{g}.\mathbf{b}^p}{2\pi}\left(1 + \frac{1}{2(1-\nu)}\right),$$

and the separation of the peaks is

$$\Delta_{obs} = \sqrt{(\Delta^2 + 4/c^2)} . \qquad (5.2)$$

In typical cases the difference between Δ_{obs} and Δ is less than 0.5 nm. The same approach can be applied for other dislocation geometries and diffracting conditions. In particular, for the case of the above disloca-

tion with $\mathbf{b} = \frac{1}{2}[1\bar{1}0]$ but in screw orientation, eqs. (5.1) and (5.2) apply with $c = -s_g/(\mathbf{g}.\mathbf{b}^p/2\pi)$.

Numerous computed images of dissociated dislocations in copper and silicon in orientations from screw to edge, and at various depths in foils of thickness from ξ_g to 6 ξ_g, have verified that the application of eq. (5.2) is useful in correcting for the small systematic difference between Δ_{obs} and Δ when $\Delta \gtrsim 2.0$ nm. For example, many-beam calculations were performed for the geometry outlined above for the $2\bar{2}0$ systematic reflections in Cu at 100 keV incident electron energy and with a nominal partial separation $\Delta = 5.0$ nm. Various thicknesses of crystal and depths of dislocation were considered. In all computed images where two image peaks were observed (and occasionally only one peak is observed due to the dependence of the peak intensity on foil thickness and dislocation depth) their separation fell within the range $\Delta_{obs} = 5.7 \pm 0.5$ nm for $s = -2.25 \times 10^{-1}$ nm^{-1}. The substitution of these values in eq. (5.2) with $\nu = 0.3$ gives $\Delta = 5.02$ nm which is in good agreement with the value $\Delta = 5.0$ nm used in the model.

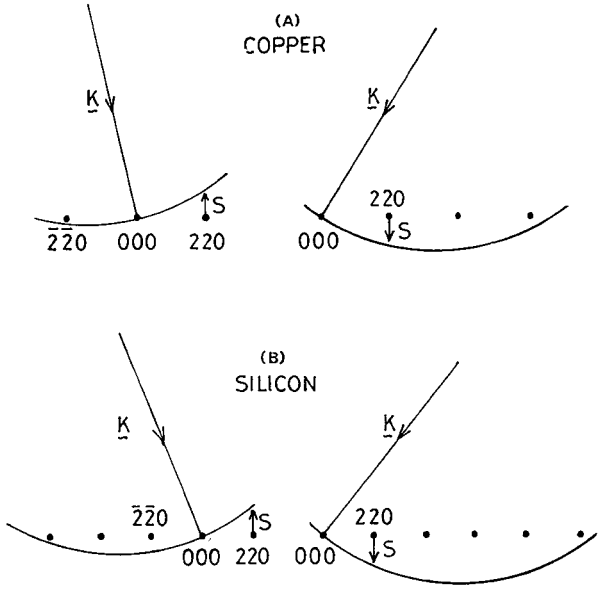

FIG. 7. — The diffracting conditions in copper (*a*) and silicon (*b*) necessary to obtain $|s_{220}| \simeq 0.2$ nm^{-1} for 100 kV electrons.

6. **Experimental details.** — To obtain weak-beam images the experimental precautions relevant to all high resolution studies are necessary i. e. the dark-field reflection must be aligned axially in the objective lens to minimise the effect of aberrations, and the image must be free from astigmatism and movement. In practice, weak-beam images require exposure times in excess of 8 (and often $\approx$ 30) seconds, and this imposes severe requirements on image and specimen stability. It also means that the image intensity is extremely weak, making focussing difficult. This difficulty can be overcome to some extent if a beam deflecting system with two or more channels is available. By arranging one channel to carry the weak-beam image and one to carry the bright-field image, the focal conditions can be set using the bright-field image. If the bright-field and weak-beam channels have both been accurately aligned, it is found experimentally that the weak-beam image is in good focus for these same focal conditions. (Of course the diffracting conditions for the two images are not the same, but this does not effect the focus.)

The general restrictions on the diffraction conditions have been discussed in § 4 primarily for the case of dislocations. It has been pointed out that the diffraction conditions chosen depend upon the accuracy required in the analysis. But the optimum conditions of the microscope capabilities are met with :

(i) $|s_g| \gtrsim 0.2$ nm^{-1} (for $\mathbf{g}.\mathbf{b} \leqslant 2$).

(ii) $|w| = |s_g \xi_g| \gtrsim 5$.

(iii) No other reflections (systematic or non-systematic) strongly excited.

To obtain a particular value of $|s_g|$ the diffracting conditions will vary for different materials and reflections. In general it can be shown geometrically that $s_g = (1 - n)\, g^2/2K$ where $K = 1/\lambda$ and the reflection ng is satisfied (where n need not be integral). For example, for 100 kV electrons in copper, an image taken with the reflection $g = 220$ has

$$g^2 = 8/(0.361)^2 \text{ nm}^{-2}$$

and $2K = (2/0.0037)$ nm^{-1}. If we require

$$s_g = \pm 0.22 \text{ nm}^{-1},$$

this results in

$$1 - n \approx \pm (0.22)/(0.11) = \pm 2 \text{ i. e. } n \approx -1 \text{ or } +3.$$

These are the diffracting conditions shown in figure 7*a*. But in the case of silicon the same value of $|s_{220}|$ requires the diffracting conditions shown in figure 7*b*. The experimental procedure is then as follows :

a) Decide which reflection g is to be used to form the weak-beam image. For the case considered in § 5, this involves determining for which $< 220 >$ reflection $\mathbf{g}.\mathbf{b} = 2$. This can be done using standard contrast techniques ([10], p. 254).

b) Determine what the Kikuchi pattern will look like when the conditions (i) and (ii) above are satisfied for the reflection g.

c) Align the microscope for high resolution microscopy for the reflection g ; e. g. rotation centre, astigmatism.

d) Tilt the specimen to obtain the correct diffraction conditions as determined in (*b*) above, with the reflection g on the optic axis.

e) Make small adjustments to the specimen orientation so that no reflections are strongly excited.

f) Attempt to focus the (weak-beam) dark-field image. If this is too difficult, use the bright-field image as discussed above.

g) Expose the plate. Do not underestimate the exposure time required : a trial image which gives an overexposure will at least show whether there is anything to be seen, and whether resolution is limited by drift, etc. Exposure times of 30 seconds are not uncommon, although 8 to 15 seconds are usually sufficient.

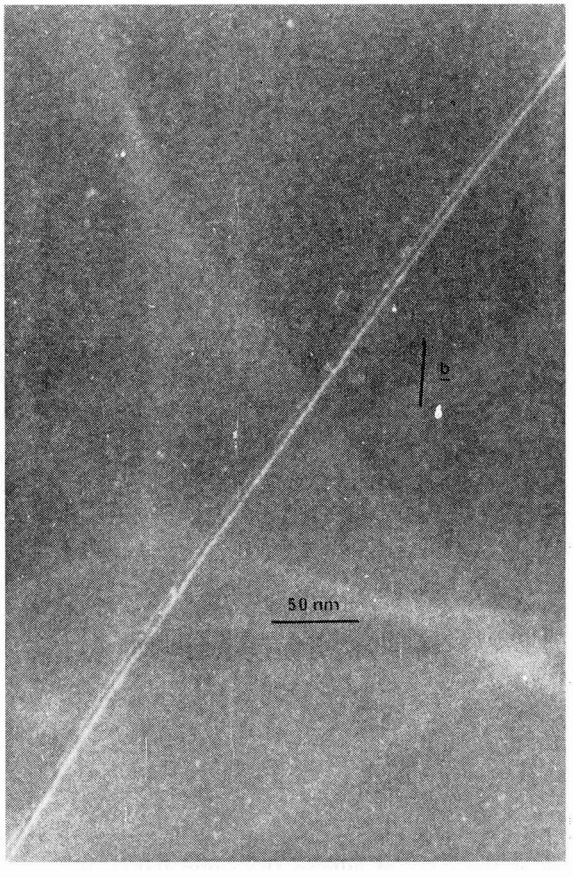

FIG. 8. — A weak-beam $2\bar{2}0$ dark-field image of a 30° dislocation in silicon. The separation of the peaks in the image is 4.8 nm, corresponding to a partial dislocation separation of 4.5 nm. (From Ray and Cockayne [25] by courtesy of the Philosophical Magazine.)

7. **Determination of γ.** — To obtain values of γ the separation of any pair of partial dislocations such as that shown in figure 8 can be used, substituting it into the equations discussed in § 5. However accuracy is gained by fitting the experimental separations for a range of dislocation line orientations with theoretical curves derived either from isotropic elasticity, or preferably from anisotropic elasticity. In figure 9, an example is shown for dissociated dislocations in silver, from which a value $\gamma = 16.3 \pm 1.7$ mJ m^{-2} was determined [17]. Values for γ in other materials determined in this way are listed in table 1.

In choosing dislocations for analysis, it is important that regions of dislocation near the foil surfaces be avoided [16]. This is because of possible influences of the surfaces not only on the separation of the partials but also on the form of the weak-beam image.

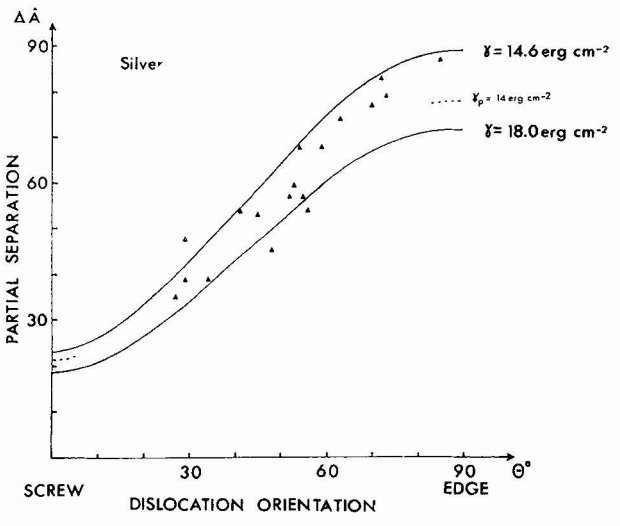

FIG. 9. — Experimental values of partial dislocation separations Δ in silver, plotted as a function of dislocation line orientation θ. The full curves are computed using anisotropic elasticity theory. The dashed lines indicate theoretical separations based on a Peierls model for the core. (From Cockayne, Jenkins and Ray [17], by courtesy of the Philosophical Magazine.)

TABLE I

Material	γ (mJ m^{-2})	Reference
Ag	16.3 ± 1.7	[17]
Cu	41 ± 9	[17]
Cu	41	[16]
Au	32 ± 5	[21]
Si	51 ± 5	[11]
Ge	60 ± 8	[22]

8. **Stackingfaults.** — 8.1 WEAK-BEAM IMAGES. — The conditions for obtaining stacking-fault contrast using large $| s_g |$ are, of course, the same as for using $s_g \approx 0$, viz $\mathbf{g}.\mathbf{R} \neq$ integer where $\mathbf{R}$ is the displacement vector of the fault. However, for inclined faults the depth periodicity of stacking-fault fringes for large $| s_g |$ is approximately $| s_g |^{-1}$. Consequently inclined faults can appear as narrow closely spaced fringes while faults lying parallel to the foil surface show contrast which is sensitive to the fault depth. For a small region of fault bounded by a partial dislocation line, the image when $s_g \approx 0$ is often dominated by the influence of the strain field of the partial. The use of large $| s_g |$ can provide a means of observing the fault image because of the diminished width of the image of the partial dislocation [12] and regions of fault $\approx$ 5 nm in size can be imaged in this way.

8.2 NATURE OF FAULTS. — To determine the nature of faults between partial dislocations (extrinsic or intrinsic) it is necessary to define the order in which the partial dislocations occur. For example, for the

case considered in § 5, a direction is assigned to the dislocation line, and the sense of **b** can then be determined by taking bright-field images under the condition $s_g > 0$. The Burgers vectors of the individual partials can then be identified by taking weak-beam images using the appropriate reflections (e. g. Fig. 1). With a knowledge of the orientation of the Thompson tetrahedron in the specimen (obtained from the Kikuchi pattern), the intrinsic or extrinsic nature of the fault can then be determined (for an example see ref [11]).

9. **Approximations.** — When using the weak-beam method to determine γ, a number of approximations in various aspects of the theories used require examination.

9.1 COLUMN APPROXIMATION. — The scattering theory used to compute the images for testing the accuracy of eq. (4.1) contains several approximations. The most important of these is the *column approximation*, and this approximation may be under severe strain for weak-beam images since the part of the image which is of most interest arises from regions close to the dislocation core. Howie and Sworn [13] have shown that images computed without the column approximation have certain features which do not appear in images computed with the column approximation. It is generally assumed that calculations performed without the column approximation will more accurately describe the experimental situation (but see [14]) and consequently the use of images calculated with the column approximation for interpreting these particular features will lead to difficulties. However at the level of resolution of experiments performed to date (e. g. partial separations $\gtrsim$ 2 nm) the calculations of Howie and Sworn [13] suggest that no important errors are introduced by this approximation (for a detailed discussion, see [15]).

9.2 ELASTICITY THEORY. — As indicated in § 7, to obtain γ from experimental measurements of r, anisotropic elasticity should be used. However to obtain r from the experimental images, a difference between the observed peak separations and the partial separations is generally allowed for by using eq. (5.2). This equation is derived using isotropic elasticity, and for anisotropic materials should be more properly derived and examined using an expression for the anisotropic strain field. Stobbs and Sworn [16] have investigated the error involved for the case of copper by computing images for both anisotropic and isotropic elasticity theory. They concluded that for copper, (i) the effect of anisotropy upon the observed peak separation, Δ_{obs}, is unimportant, and (ii) the relationship between Δ_{obs} and Δ given by eq. (5.2) is accurate to better than 10 %.

9.3 EFFECT OF CORE STRUCTURE. — The ability of the weak-beam method to resolve Shockley partial dislocations having separations approaching 2 nm means that the influence of dislocation cores may become appreciable. The experimental curve of partial separation as a function of dislocation line orientation proves of particular interest for copper, because in this material the Shockley partials have a separation of approximately 2 nm near screw orientation. At such a separation, there is the possibility that overlap of the dislocation cores may produce deviations from separations predicted by continuum elasticity theory using unextended cores. Indeed the experimental results led to the observation that the value of γ deduced from the partial separations could be sensitive to the dislocation core model used [17]. The deviations from continuum elasticity theory should be most appreciable for dislocations near screw orientation, and suggestions of a deviation of the experimental values near screw orientation from those predicted by anisotropic elastic continuum theory have been detected [16]. The possibility of interpreting these experimental results in terms of particular core models has been discussed [18, 19, 20], and the influence of core models on the value of γ obtained from a particular partial separation has been investigated [20]. From this last study it was deduced that the core structure of partial dislocations could lead to either a larger or smaller separation than the separation, r_0, expected for the partials if they were regarded as singular dislocations, depending on the core parameters. This effect may become very pronounced if the width of the cores is comparable with $r_0/2$. For example, in the framework of the model used in the study, and assuming reasonable values of the core parameters, it was shown that the stacking-fault energy in Cu derived from the measured partial separation could be between 31 and 50 mJ m^{-2}.

10. **Discussion.** — In this paper, only the dissociation of Shockley partials has been discussed in any detail. The closely related case of the dissociation of superlattice dislocation in ordered alloys has been studied both for twofold [23] and fourfold [24] dissociations. The latter case involves measuring the separations of superlattice dislocations and the determinations of two antiphase boundary energies, and the experimental procedure and analysis, using weak-beam images, is particularly interesting.

Many other arrangements of interacting dislocations and small defects suggest themselves as amenable to the determination of stacking-fault energies using weak-beam images. With brighter electron sources, the use of larger values of $| s_g |$ will be possible, and more accurate measurements may result. However, even with present measurements, the influence of core structures effects the value of γ determined from the experimentally measured partial separations. This becomes particularly important for separations $\lesssim$ 2.0 nm, but for such small separations many other approximations in the analysis become important.

References

[1] COCKAYNE, D. J. H., RAY, I. L. F. and WHELAN, M. J., *Phil. Mag.* **20** (1969) 1265.

[2] READ, W. T., *Dislocations in Crystals* (Wiley : New York) 1953.

[3] HUMBLE, P., *Modern Imaging and Diffraction Techniques in Materials Science* (North Holland : Amsterdam) 1970.

[4] WHELAN, M. J., *Proc. R. Soc.* A **249** (1958) 114.

[5] BROWN, L. M., *Phil. Mag.* **10** (1964) 441.

[6] COCKAYNE, D. J. H., *Z. Naturforsch.* **27a** (1972) 452.

[7] HIRSCH, P. B., HOWIE, A. and WHELAN, M. J., *Phil. Trans. Roy. Soc.* A **252** (1960) 499.

[8] DE RIDDER, R. and AMELINCKX, S., *Phys. Stat. Sol.* (b) **43** (1971) 541.

[9] WILKENS, M. and HORNBOGEN, E., *Phys. Stat. Sol.* **4** (1964) 557.

[10] HIRSCH, P. B., HOWIE, A., NICHOLSON, R. B., PASHLEY, D. W. and WHELAN, M. J., *Electron Microscopy of Thin Crystals* (Butterworths : London) 1965.

[11] RAY, I. L. F. and COCKAYNE, D. J. H., *Proc. R. Soc.* A **325** (1971) 543.

[12] COCKAYNE, D. J. H., JENKINS, M. L., RAY, I. L. F. and WHELAN, M. J., Proc. 25th Anniv. Meeting of EMAG, Cambridge, 1971, p. 108.

[13] HOWIE, A. and SWORN, C. H., *Phil. Mag.* **22** (1970) 861.

[14] WILKENS, M. and KATERBAU, K. H., Proc. 5th European Congress on Electron Microscopy, Manchester, 1972, p. 414.

[15] HOWIE, A., *Modern Imaging and Diffraction Techniques in Materials Science* (North Holland : Amsterdam) 1970.

[16] STOBBS, W. M. and SWORN, C. H., *Phil. Mag.* **24** (1971) 1365.

[17] COCKAYNE, D. J. H., JENKINS, M. L. and RAY, I. L. F., *Phil. Mag.* **24** (1971) 1383.

[18] NORGETT, M. J., PERRIN, R. C. and SAVINO, E. J., *J. Phys. F* **2** (1972) L 73.

[19] PERRIN, R. C. and SAVINO, E. J., *J. Microsc.* **98** (1973) 214.

[20] COCKAYNE, D. J. H. and VITEK, V., *Phys. Stat. Sol.* (b) **65** (1974) 751.

[21] JENKINS, M. L., *Phil. Mag.* **26** (1972) 747.

[22] RAY, I. L. F. and COCKAYNE, D. J. H., *J. Microsc.* **98** (1973) 170.

[23] RAY, I. L. F., CRAWFORD, R. C. and COCKAYNE, D. J. H., *Phil. Mag.* **21** (1970) 1027.

[24] CRAWFORD, R. C., RAY, I. L. F. and COCKAYNE, D. J. H., *Phil. Mag.* **27** (1973) 1.

[25] RAY, I. L. F. and COCKAYNE, D. J. H., *Phil. Mag.* **22** (1970) 853.